MCB
Journals.ASM.org

# STIM1-$Ca^{2+}$ Signaling Is Required for the Hypertrophic Growth of Skeletal Muscle in Mice

**Tianyu Li,[a,b,c] Elizabeth A. Finch,[a,c] Victoria Graham,[a,c] Zhu-Shan Zhang,[a,b,c] Jin-Dong Ding,[d] Jarrett Burch,[a,c] Masatsugu Oh-hora,[e] and Paul Rosenberg[a,b,c]**

Department of Medicine,[a] Sarah W. Stedman Nutrition and Metabolism Center,[b] Ion Channel Research Group,[c] and Department of Ophthalmology, Eye Center,[d] Duke University School of Medicine, Durham, North Carolina, USA, and Department of Cell Signaling, Graduate School Tokyo Medical and Dental University, Tokyo, Japan[e]

**Immediately after birth, skeletal muscle must undergo an enormous period of growth and differentiation that is coordinated by several intertwined growth signaling pathways. How these pathways are integrated remains unclear but is likely to involve skeletal muscle contractile activity and calcium ($Ca^{2+}$) signaling. Here, we show that $Ca^{2+}$ signaling governed by stromal interaction molecule 1 (STIM1) plays a central role in the integration of signaling and, therefore, muscle growth and differentiation. Conditional deletion of STIM1 from the skeletal muscle of mice (mSTIM1$^{-/-}$ mice) leads to profound growth delay, reduced myonuclear proliferation, and perinatal lethality. We show that muscle fibers of neonatal mSTIM1$^{-/-}$ mice cannot support the activity-dependent $Ca^{2+}$ transients evoked by tonic neurostimulation, even though excitation contraction coupling (ECC) remains unperturbed. In addition, disruption of tonic $Ca^{2+}$ signaling in muscle fibers attenuates downstream muscle growth signaling, such as that of calcineurin, mitogen-activated protein (MAP) kinases, extracellular signal-regulated kinase 1 and 2 (ERK1/2), and AKT. Based on our findings, we propose a model wherein STIM1-mediated store-operated calcium entry (SOCE) governs the $Ca^{2+}$ signaling required for cellular processes that are necessary for neonatal muscle growth and differentiation.**

Stromal interaction molecule 1 (STIM1) is a single-pass transmembrane protein located in the sarcoplasmic reticulum (SR)/endoplasmic reticulum (ER), where it functions as the $Ca^{2+}$ sensor and activates $Ca^{2+}$ entry by the Orai channels (14, 22, 31). While the function of STIM1-SOCE has been well characterized in nonexcitable cells, the putative role for STIM1 in skeletal muscle has only recently been recognized. Recent studies have shown that when SOCE is eliminated, myotubes display defects in fusion, growth, and differentiation (3), and the mice exhibit impaired skeletal muscle growth and reduced perinatal survival (16, 27, 29). Furthermore, human patients harboring mutations in either STIM1 or Orai1 not only manifest profound immune deficiency but also exhibit signs of a congenital skeletal myopathy and hypotonia (8, 18). Together, these findings strongly suggest an important role for STIM1-SOCE in the regulation of skeletal muscle growth and function. Clearly, a skeletal muscle-specific STIM1 knockout mouse model would provide a direct way to address this hypothesis and to explore the underlying mechanisms.

In the present work, we generated a skeletal muscle-specific STIM1 knockout mouse using Cre-Lox technology to understand the role of STIM1 in skeletal muscle. We demonstrate that in skeletal muscle, STIM1 is necessary to maintain both basal cytosolic $Ca^{2+}$ levels and the $Ca^{2+}$ content of the SR stores. We suggest that STIM1 acts as an ER/SR $Ca^{2+}$ sensor in skeletal muscle, as it does in other cells, where it coordinates $Ca^{2+}$ homeostasis through a relationship with extracellular $Ca^{2+}$ sources. Disruption of STIM1-SOCE resets the $Ca^{2+}$ equilibrium of myofibers, which impairs their ability to respond to locomotor stress associated with postnatal life. While these changes in cytosolic and SR $Ca^{2+}$ levels did not significantly alter $Ca^{2+}$ release events evoked by a single action potential (excitation contraction coupling [ECC]), we show attenuation of $Ca^{2+}$ signals following tonic stimulation of mSTIM1$^{-/-}$ muscles. Corresponding to these changes in repetitive $Ca^{2+}$ signals, mSTIM1$^{-/-}$ muscles exhibit a reduction in the activation status of $Ca^{2+}$-dependent signal transduction pathways, including calcineurin, mitogen-activated protein (MAP) kinase, extracellular signal-regulated kinase 1 and 2 (ERK1/2), and AKT. Given the importance of these signaling pathways to muscle maturation growth, we propose that muscle lacking STIM1 failed to activate these signaling pathways during the first weeks of postnatal life, resulting in limited muscle growth and neonatal lethality. Together, these findings indicate that STIM1 acts as a regulator of skeletal muscle $Ca^{2+}$ signaling, where it provides the $Ca^{2+}$ entry necessary to control $Ca^{2+}$-dependent gene expression and growth signaling in skeletal muscle.

## MATERIALS AND METHODS

**Animals.** STIM1$^{flox/flox}$ mice (C57BL/6) were generated as previously described (16). Myogenin (skeletal muscle specific)-Cre transgenic mice (Myo-Cre) (C57BL/6) were obtained from Eric Olson (13). To generate a skeletal muscle knockout of STIM1, Myo-Cre transgenic mice were bred with founder STIM1$^{flox/flox}$ mouse and the progeny STIM1$^{flox/-}$ Myo-Cre$^{+/-}$ were bred with STIM1$^{flox/flox}$ mice. Wild-type (WT) animals consisted of STIM1$^{flox/flox}$ mice. All mice were maintained in pathogen-free barrier facilities at Duke University and were used in accordance with protocols approved by the Division of Laboratory Animal Resources and Institutional Animal Care & Use Committee at Duke University.

**Primary cultured myotubes and isolation of FDB fiber.** Primary myoblasts were isolated from STIM1 WT and mSTIM1$^{-/-}$ neonates by collagenase digestion using a previously described protocol (28) and subsequently differentiated into myotubes in differentiating medium (HIT medium). Differentiating medium contained Dulbecco's modified Ea-

Received 22 November 2011 Returned for modification 25 January 2012
Accepted 14 May 2012
Published ahead of print 29 May 2012
Address correspondence to Paul Rosenberg, rosen029@mc.duke.edu.

doi:10.1128/MCB.06599-11

gle's medium (DMEM)-high glucose, 2% house serum, 10 μg/ml transferrin, 10 μg/ml insulin, 50 mM HEPES buffer, pH 7.4, 100 U/ml penicillin-streptomycin. Primary myotubes were used for experiments after 5 days in differentiation medium. Each experiment was conducted with a minimum of 4 or 5 animals. Flexor digitorum brevis (FDB) fibers were isolated from juvenile STIM1 WT and mSTIM1$^{-/-}$ mice following the protocol described in reference 25.

**Adenovirus overexpression in primary cultured myotubes.** Primary cultured myotubes were rinsed in Hanks' balanced salt solution (HBSS) and incubated with control (LacZ) or constitutively active calcineurin adenovirus (multiplicity of infection [MOI] of 50) in 1 ml of HBSS for 3 h at 37°C. Then, 2 ml of HIT medium was added to the wells for an additional 12 h at 37°C. Virus was then removed, and cells were rinsed with HBSS and incubated with HIT medium for 48 h before lysis for immunoblot analysis.

**Calcium imaging of myotubes and FDB myofibers.** To monitor cellular $Ca^{2+}$ concentration ($[Ca^{2+}]_c$), myotubes or myofibers were loaded with Fura-2-acetoxymethyl ester (1 μM; Molecular Probes/Invitrogen) for 30 min at room temperature, washed, and incubated for 30 min in dye-free buffer. For myotubes, incubations and washes were carried out in Ringer solution (140 mM NaCl, 2.8 mM KCl, 2 mM $CaCl_2$, 2 mM $MgCl_2$, 10 mM glucose, and 10 mM HEPES, pH 7.4). For myofibers, incubations were carried out in Opti-MEM with 10% horse serum and washes were carried out in Ringer solution. For fluorescence imaging, myotube cultures or myofibers plated on collagen were mounted on a Nikon TE2000 inverted microscope equipped with a Photometrics CoolSnap camera, a xenon arc lamp, and a lambda DG-4 rapid filter changer (Sutter). Image acquisition was controlled using Metafluor/Metamorph software (Molecular Devices). Images were acquired using a 40× S Plan 1.3-numerical-aperture (NA) objective lens for myotubes and field stimulation of myofibers and a 20× Plan Fluor 0.5-NA objective lens for myofibers. Fura-2 fluorescence was measured by alternate excitation at 340 and 380 nm and emission at 510 nm. For measurements under basal conditions and during SOCE, images were acquired every 3 s. For measurements during field stimulation, 340/380 image pairs were acquired every 750 ms. All experiments were carried out at room temperature. For myotube experiments, cultures were perfused with $Ca^{2+}$-containing Ringer or $Ca^{2+}$-free Ringer. For myofiber experiments, fibers were perfused with oxygenated $Ca^{2+}$-containing solution (120 mM NaCl, 5 mM KCl, 2 mM $CaCl_2$, 1 mM $MgCl_2$, 25 mM $NaHCO_3$, 1 mM $NaH_2PO_4$, and 10 mM glucose, pH 7.4), $Ca^{2+}$-free solution (120 mM NaCl, 5 mM KCl, 1 mM $MgCl_2$, 25 mM $NaHCO_3$, 1 mM $NaH_2PO_4$, and 10 mM glucose, pH 7.4), or $Ba^{2+}$-containing solution (120 mM NaCl, 5 mM KCl, 2 mM $BaCl_2$, 1 mM $MgCl_2$, 25 mM $NaHCO_3$, 1 mM $NaH_2PO_4$, and 10 mM glucose, pH 7.4) containing 25 μM BTS (*N*-benzyl-*p*-toluene sulfonamide; Sigma) to limit muscle contraction.

SOCE was measured by subjecting myofibers to a standard SOCE protocol (27). $Ca^{2+}$ stores were depleted using either cyclopiazonic acid (CPA; 30 μM) alone or CPA plus 10 mM caffeine. SOCE was measured using $Ba^{2+}$ as a surrogate for $Ca^{2+}$ because $Ba^{2+}$ is less readily buffered or sequestered than $Ca^{2+}$. Image processing and analysis were performed using Metafluor/Metamorph software (Molecular Devices). To measure $[Ca^{2+}]_c$, the average, background-subtracted Fura-2 intensity at 340 nm and 380 nm in regions of interest was used to calculate the 340/380 ratio. The maximum slope of the rise in cytosolic $Ca^{2+}$ levels following reintroduction of $Ba^{2+}$ provides a quantitative measure of SOCE. The integrated area of the CPA- or CPA-caffeine-mediated $Ca^{2+}$ transient provides a measure of $Ca^{2+}$ store content. The magnitude and kinetics of the rise in $[Ca^{2+}]_c$ following reintroduction of $Ba^{2+}$ provide a quantitative measure of SOCE.

**Field stimulation.** Electrical field stimulation of myofibers was delivered via a 35-mm dish insert with a pair of platinum electrodes lining the perfusion trough (RC-37FS; Warner Instruments), and the electrical stimulus was generated by an A310 Accupulser (World Precision Instruments) and an A385 Stimulus Isolator (World Precision Instruments) connected to the dish insert. Bursts of stimulation, each of which is called a "'stimulus" hereinafter, consisted of 1-ms current pulses (100 mA) applied at 50 Hz for the indicated stimulus duration. The stimulus-response curve was generated by applying such stimuli at a range of stimulus durations (100 ms to 2 s), with a single test stimulus applied every 50 s. Trains of stimuli were generated by applying a 2-s stimulus every 5 s for the indicated train duration. For electrical stimulation of hind limbs, hind limbs were perfused with oxygenated $Ca^{2+}$-containing myofiber solution and trains of stimuli were generated by applying a 500-ms stimulus every 5 s for 30 min in the presence of insulin (10 μg/ml). The controls were hind limbs from the same animal that were maintained in oxygenated solution for 30 min.

**Recording voltage-gated $Ca^{2+}$ currents.** $Ca^{2+}$ currents were recorded using the ruptured whole-cell patch-clamp technique. The patch pipettes (borosilicate glass) had a resistance of 4 to 6 MΩ. The liquid junction potential was nulled before gigiseal formation. Whole-cell currents were recorded using an AXON AXOPatch 200B amplifier connected to a DIGIDATA 1320A digital converter. Whole-cell currents were collected using PClampex software 9.0 (Molecular Devices). All experiments were carried out at room temperature using the Ringer solutions described above. The voltage protocol to elicit calcium current ($I_{Ca}$) involved a test potential of 10 mV for 250 ms from a holding potential of −40 mV.

**Immunohistochemistry.** Muscles were isolated from appropriately aged mice, mounted in O.C.T. (optimal cutting embedding medium) with gum tragacanth (at a 4:1 ratio), and flash frozen in an isopentane bath suspended in liquid nitrogen. Samples were stored at −80°C until being sectioned. Cross sections of muscle were cut from the belly of the muscle at day 21 of postnatal life (P21) or the whole leg at P1 at a thickness of 14 μm. Sections were fixed with 4% PFA for 30 min or ice-cold acetone (for dystrophin staining) for 10 min. For myofiber counts and cell size determination, cryosections were stained with hematoxylin and eosin. The primary antibodies used were dystrophin at a dilution of 1:1,000 (Sigma-Alderich) and Pax7 (Hybridoma) at a dilution of 1:100. Staining was visualized using anti-mouse antibody–Alexa Fluor 555. All sections were counterstained with DAPI (4′,6′-diamidino-2-phenylindole) and mounted in Vectashield (Vector labs).

**Immunoblotting.** Standard protocols were used for immunoblot analysis. Blots were incubated overnight at 4°C with antibodies. Antibodies against STIM1 (MA1-19451) and NFATC1 were from Affinity BioReagents (MA3-024). Mouse monoclonal antibody to GAPDH (glyceraldehyde-3-phosphate dehydrogenase) and rabbit polyclonal antibody to β-actin were from Abcam (ab8245 and ab8227, respectively). Anti-Erk1/2, -phospho-Erk1/2, -phospho-AKT (Ser473), -AKT, -phospho-p38, and -p38 were from Cell Signaling Technology (9102, 9106, 9271, 9272, 4511, and 9212, respectively). Antimyoglobin antibody was from Abgent (AJ1520a), and anti-SERCA1 antibody was from Pierce (VE121G9). Antibodies against MEF-2 (sc-313) and peroxisome proliferator-activated receptor β/δ (PPAR-β/δ; (sc-1987) were from Santa Cruz Biotechnology, Inc. PGC-1α antibody was from Calbiochem (ST1202). Signals were detected using horseradish peroxidase (HRP)-conjugated secondary antibody and the ECL Western blotting system (Amersham Biosciences, Piscataway, NJ) and quantified with the VersaDoc Imaging System (Bio-Rad).

**Electron microscopy.** Mice were deeply anesthetized with sodium pentobarbital and perfused transcardially with fixative (a mixture of freshly prepared 2% paraformaldehyde and 2% glutaraldehyde in 0.1 M phosphate buffer, pH 7.4). Tibialis anterior muscles were dissected and postfixed in the same fixative overnight at 4°C. Small pieces of tissue of ~1 mm were cut and fixed in 1% osmium tetraoxide, stained *en bloc* with 1% uranyl acetate, dehydrated in a graded ethanol series followed by propylene oxide, and infiltrated and embedded with a mixture of Epon and Spurr resins. Thin sections of ~60 nm were mounted on copper grids and counterstained with 2% uranyl acetate and Sato's lead. Sections were examined under a FEI Tecnai twin electron microscope. Images were ac-

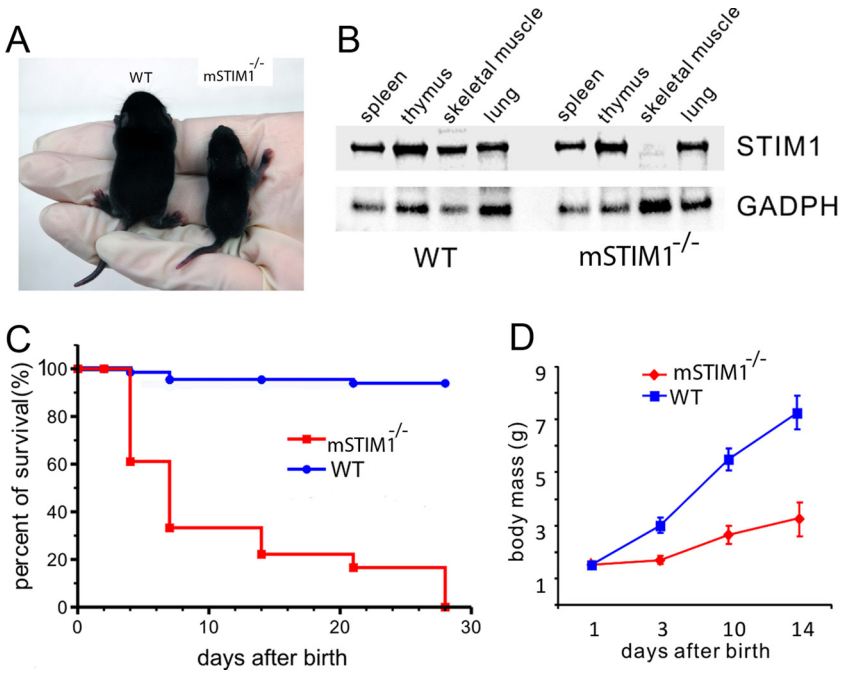


**FIG 1** Skeletal muscle-specific deletion of STIM1. (A) Photograph of mouse (P14) lacking STIM1 in skeletal muscle. Mice were generated by crossing STIM1 exon 1-floxed mice with mice carrying Cre recombinase under the control of the myogenin promoter. (B) Protein lysates prepared from mSTIM1$^{-/-}$ and WT mice were immunoblotted for STIM1 using a polyclonal antibody. (C) Kaplan-Meyer curves for survival of WT ($n = 66$) and mSTIM1$^{-/-}$ ($n = 18$) mice. (D) Growth curves for mSTIM1$^{-/-}$ mice reveal severe growth failure after postnatal day 3 (P3). $n = 30$ for each genotype.

quired with a Tecnia Imaging and Analysis charge-coupled-device (CCD) camera.

**Statistical analysis.** The numbers of mice used in experiments for each study are indicated in figure legends. Values are presented as means ± standard errors of the means (SEM). A two-tailed Student's *t* test was used to calculate *P* values.

## RESULTS

**Skeletal muscle-specific deletion of STIM1.** To understand the role of STIM1 in skeletal muscle, we generated skeletal muscle-specific STIM1 null mice (mSTIM1$^{-/-}$) (Fig. 1A) by crossbreeding mice in which exon 2 of the *Stim1* gene was floxed with LoxP sites (16) and transgenic mice carrying a myogenin-Cre transgene (13). We verified that STIM1 is specifically eliminated from skeletal muscle, as shown by the experiment whose results are presented in Fig. 1B, where STIM1 protein was not detected in skeletal muscle from mSTIM1$^{-/-}$ mice but was abundantly expressed in all other tissues examined. The mSTIM1$^{-/-}$ mice exhibited normal Mendelian ratios during embryonic development (not shown) but significant perinatal lethality during the first 4 weeks of life (Fig. 1C). Further characterization of the mSTIM1$^{-/-}$ mice revealed a profound reduction in whole-body mass compared to that of age-matched WT mice (Fig. 1D). The results of these morphometric studies provide strong evidence that STIM1 in skeletal muscle has a critical role in whole-body growth, which is consistent with previous findings for mice with global deletions of STIM1 and Orai1 (27, 29).

To define how STIM1 influenced muscle growth, we first analyzed myofiber number and size in WT and mSTIM1$^{-/-}$ mice using hematoxylin and eosin staining, as well as dystrophin immunostaining, to define individual fibers. At 3 weeks of age (P21), the muscle fiber numbers were comparable between WT and mSTIM1$^{-/-}$ mice (WT, 932.3 ± 20.5, and mSTIM1$^{-/-}$, 937.3 ± 10.6), thus excluding defective myofiber proliferation as a cause for the reduced muscle mass of mSTIM1$^{-/-}$ mice (Fig. 2A). To compare fiber size between WT and mSTIM1$^{-/-}$ muscles, the cross-sectional area (CSA) was determined in muscle cryosections from P1 and P21 mice. In fact, no differences in CSA were observed for muscles from newborn (P1) WT and mSTIM1$^{-/-}$ mice (WT, 145.0 ± 5.2 $\mu m^2$, and mSTIM1$^{-/-}$, 145.9 ± 5.7 $\mu m^2$). However, the CSA and, therefore, fiber size of P21 mSTIM1$^{-/-}$ muscles were dramatically reduced compared to those of WT muscles (WT, 953.0 ± 16.4 $\mu m^2$, and mSTIM1$^{-/-}$, 486.9 ± 12.3 $\mu m^2$) (Fig. 2B to F).

Postnatal muscle growth occurs by both the addition of satellite cells, resulting in the increase in myonuclei, and expansion of nonnuclear elements, including myofibrils, sarcoplasmic reticulum, and mitochondria. To ascertain whether the satellite cell number is normal in mSTIM1$^{-/-}$ muscles, we analyzed Pax7-positive myonuclei from cryosections of P21 WT and mSTIM1$^{-/-}$ mice. No significant differences were observed in the percentages of Pax7-positive nuclei per myonucleus for WT and mSTIM1$^{-/-}$ muscles (WT, 5.6 ± 0.07, and mSTIM1$^{-/-}$, 6.1 ± 0.2), indicating that mSTIM1$^{-/-}$ muscle maintained satellite cell ratios (Fig. 2G to I). To determine whether satellite cell proliferation or myonuclear accretion was altered by deletion of STIM1, we compared the number of myonuclei per muscle section for WT and mSTIM1$^{-/-}$ mice at P1 and P21. Newborn (P1) mice exhibited a similar number of myonuclei per muscle fiber section (WT, 1.07 ± 0.01, and mSTIM1$^{-/-}$, 1.08 ± 0.04); however, at P21, the number of myonuclei per fiber section was markedly reduced in mSTIM1$^{-/-}$ mice (WT, 3.6 ± 0.15, and mSTIM1$^{-/-}$, 2.6 ± 0.1) (Fig. 2J).

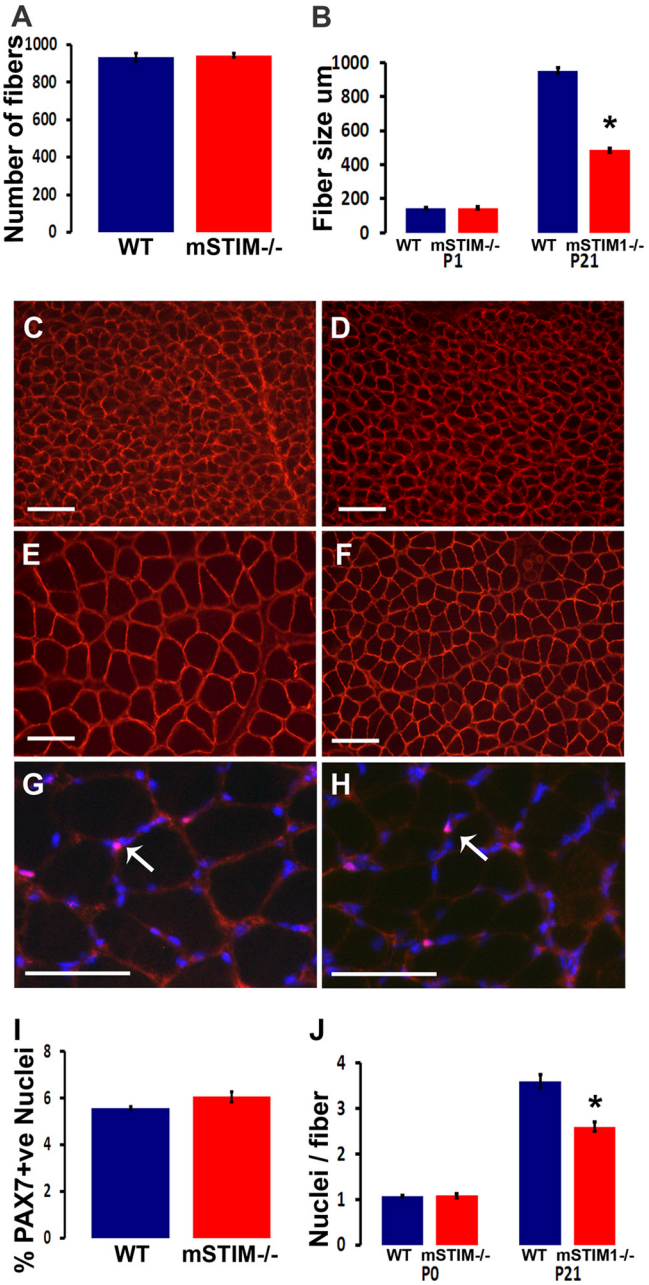


**FIG 2** Skeletal muscle-specific deletion of STIM1 limits skeletal muscle growth. (A) Fiber numbers in WT and mSTIM1$^{-/-}$ mice at P21. (B) Myofiber sizes ($\mu m^2$) in P1 and P21 mice. (C to F) Demonstration of fiber size using dystrophin staining (red) of cross sections of WT and mSTIM1$^{-/-}$ skeletal muscle at P1 and P21. (C) WT at P1, (D) mSTIM1$^{-/-}$ at P1, (E) WT at P21, (F) mSTIM1$^{-/-}$ at P21. (G and H) PAX7 (red) labeling of satellite cell nuclei in WT (G) and mSTIM1$^{-/-}$ (H) muscle cross sections at P21. Nuclei are labeled with DAPI (blue). (I) Percentages of Pax 7-positive (+ve) nuclei at P21. (J) Numbers of nuclei per fiber cross section at P1 and P21. Data shown represent the means ± SEM. *, $P < 0.01$. $n = 3$. Scale bars = 50 μm.

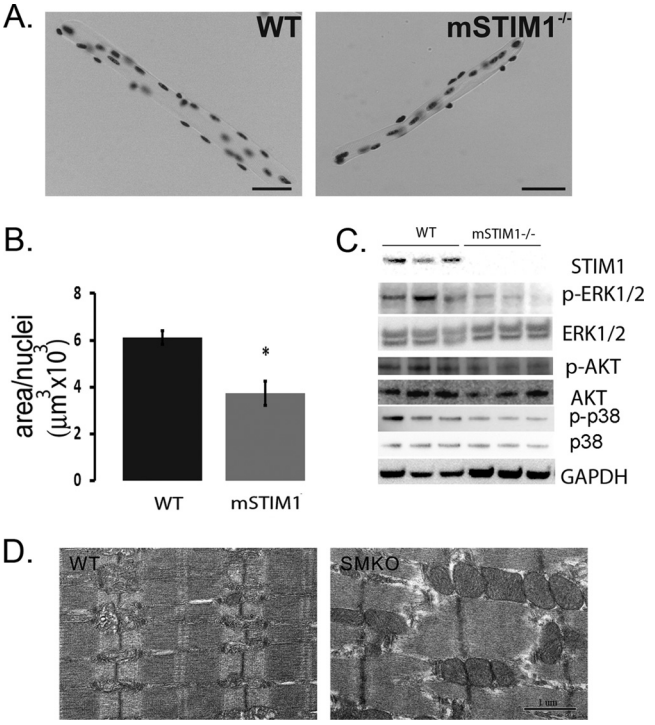


**FIG 3** Reduced myonuclear domain and altered ultrastructure in WT and mSTIM1$^{-/-}$ skeletal muscle. (A) Representative images of WT and mSTIM1$^{-/-}$ FDB fibers stained with DAPI, for the measurement of myonuclear domain size. Scale bar = 50 μm. (B) Comparison of myonuclear domain (total fiber volume/myonuclei) in FDB fibers from WT and mSTIM1$^{-/-}$ littermates at P21 ($n = 3$). Data shown represent the means ± SEM. *, $P < 0.05$. (C) Immunoblotting for STIM1, p-ERK1/2, ERK1/2, p-AKT, AKT, p-p38, p38, and GAPDH in three pairs of WT and mSTIM1$^{-/-}$ muscles. (D) Transmission electron micrographs of hind-limb muscles from P10 WT and mSTIM1$^{-/-}$ (SMKO) mice.

While our results to this point indicate that myonuclear proliferation during neonatal myogenesis was limited in mSTIM1$^{-/-}$ mice, it is also possible that nonnuclear elements failed to expand in these muscle fibers. In fact, given the relationship between the myonucleus and the volume of myofiber surrounding it, or the myodomain, we considered the possibility that failed expansion of the myodomain may account for the reduced muscle mass of mSTIM1$^{-/-}$ mice. To further test this idea, we quantified the myodomain from isolated single muscle fibers from the flexor digitorum brevis (FDB) muscle of WT and mSTIM1$^{-/-}$ mice. We found that the number of nuclei per volume of myofiber was significantly reduced in the muscle lacking STIM1 (WT, $6.1 \pm 5.2 \times 10^3$ $\mu m^3$, and mSTIM1$^{-/-}$, $145.9 \pm 5.7 \times 10^3$ $\mu m^3$) (Fig. 3A and B). When considered together, the results of these studies indicate that the muscles of mSTIM1$^{-/-}$ mice manifest defects in myonuclear proliferation and myodomain expansion. As a result, mSTIM1$^{-/-}$ mice exhibit a profound defect in skeletal muscle maturation and growth which limits muscle mass and neonatal survival.

We next investigated the activation status of several signaling pathways known to govern the maturational growth of skeletal muscle (Fig. 3C). ERK1/2 activity, as indicated by its phosphorylation state (p-ERK1/2), was found to be markedly diminished, as evidenced by the reduced p-ERK1/2 levels in muscles of mSTIM1$^{-/-}$ mice (4, 20) (Fig. 3C). We also show that the activation status of both p38 MAP kinase and AKT were diminished in the muscles of mSTIM1$^{-/-}$ mice, as detected by the reduced phosphorylation of p38 and AKT (Fig. 3C). Given that p38 and AKT signaling have critical roles in muscle growth and differentiation

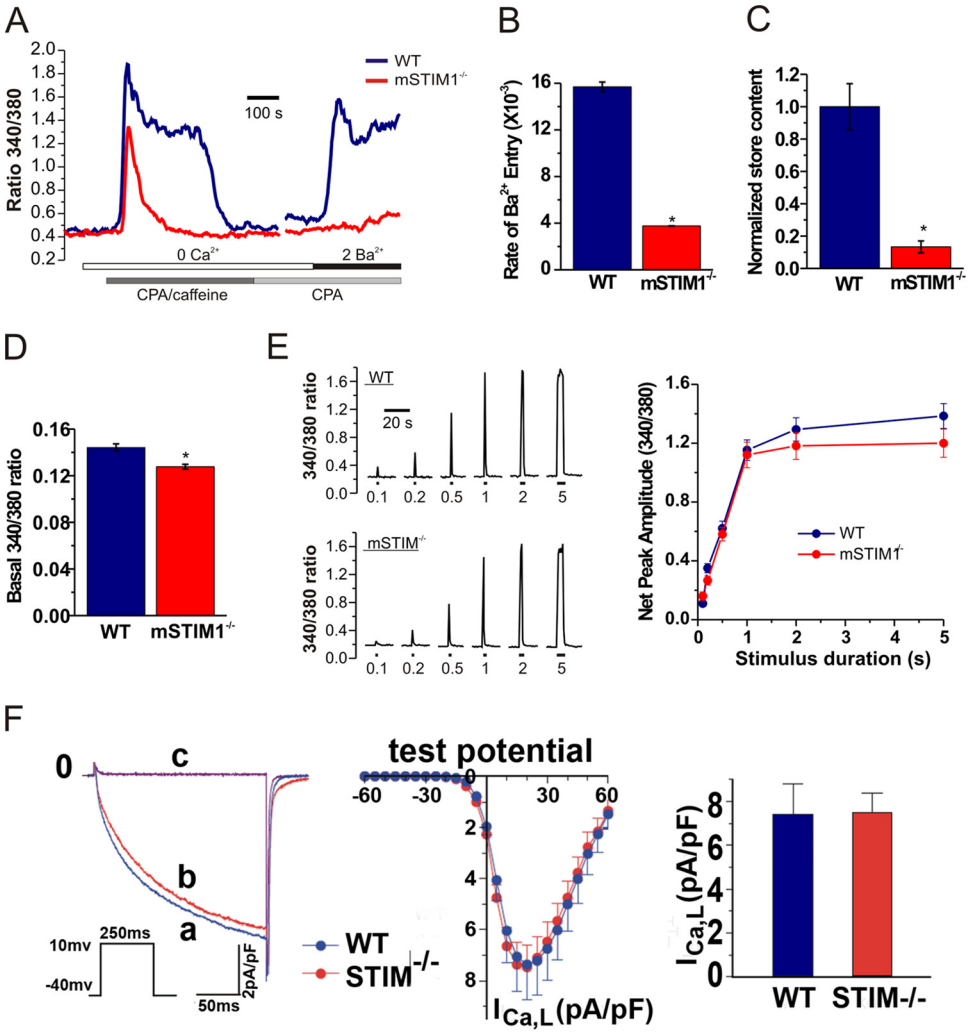


**FIG 4** Abnormalities of $Ca^{2+}$ signaling in mSTIM1$^{-/-}$ muscle fibers. $Ca^{2+}$ signals were measured in single FDB myofibers from WT and mSTIM1$^{-/-}$ mice using Fura-2. (A) Store-operated calcium entry (SOCE) in WT and mSTIM1$^{-/-}$ fibers. Representative traces from individual myofibers illustrate a significant decrease in SOCE in mSTIM1$^{-/-}$ myofibers compared to that in myofibers from WT littermates. (B) The rate of SOCE, calculated by the first derivative of the 340-/380-nm ratio during the maximal rate of rise of the $Ca^{2+}$ increase, was significantly higher in WT myofibers ($n = 15$) than in mSTIM1$^{-/-}$ myofibers ($n = 9$). *, $P < 0.005$. (C) The relative $Ca^{2+}$ store contents were determined for WT ($n = 15$; from 2 mice) and mSTIM1$^{-/-}$ ($n = 18$; from 2 mice) myofibers. *, $P < 0.0005$. (D) Relative basal $Ca^{2+}$ levels in WT ($n = 62$; 3 mice) and mSTIM1$^{-/-}$ ($n = 61$; 4 mice) myofibers. Images of 10 fields of myofibers were obtained from each dish. (E) ECC was evaluated by monitoring $Ca^{2+}$ signals produced in myofibers by electrical field stimulation. Left, representative $Ca^{2+}$ responses to stimulus bursts of different durations (100 ms to 5 s at 50 Hz) in WT and mSTIM1$^{-/-}$ fibers. Right, stimulus-response plot of average $Ca^{2+}$ transient amplitudes versus burst duration in WT ($n = 26$) and mSTIM1$^{-/-}$ myofibers ($n = 22$). (F) $Ca^{2+}$ currents ($I_{Ca}$s) were measured using patch clamp recording from WT ($n = 9$; from 3 mice) and mSTIM1$^{-/-}$ ($n = 15$; from 4 mice) myotubes. $I_{Ca}$s were elicited by a test potential of 10 mV for 250 ms from a holding potential of −40 mV (left). Current-voltage relationship of $I_{Ca}$ in myotubes from WT and mSTIM1$^{-/-}$ myotubes (middle). Summary data are provided for WT and mSTIM1$^{-/-}$ myotubes (right). pA/pF, inward current amplitude normalized to cell capacitance.

(21), these findings from mSTIM1$^{-/-}$ muscles are consistent with a defect in skeletal muscle growth and raise the possibility that STIM1 acts upstream of several myogenic signaling pathways. Finally, we examined electron micrographs of skeletal muscle sections from P10 WT and mSTIM1$^{-/-}$ mice and found markedly distorted muscle architecture, including swollen mitochondria (Fig. 3D), that strongly resembles defects observed in the muscle ultrastructure of mice from globally STIM1 null mice (27). When taken together, these data show that the reduced muscle mass and lethality observed in mice lacking skeletal muscle STIM1 results from abnormalities in myonuclear proliferation and myodomain expansion; moreover, the activation states of several signal transduction pathways associated with muscle growth were limited.

**$Ca^{2+}$ signaling in mSTIM1$^{-/-}$ muscle fibers.** To understand how deletion of STIM1 influences $Ca^{2+}$ signaling to mature muscle fibers, we conducted a series of $Ca^{2+}$-imaging experiments on single muscle fibers isolated from the FDB muscles of WT and mSTIM1$^{-/-}$ mice (Fig. 4). FDB fibers were subjected to a store depletion protocol to assess the extent of $Ca^{2+}$ releasable from the SR and activate SOCE by the RYR1 agonist caffeine and the SERCA1 inhibitor cyclopiazonic acid (CPA). We found that SOCE was nearly absent in fibers from mSTIM1$^{-/-}$ mice compared to the robust $Ca^{2+}$ entry in WT fibers. We also found that depletion of $Ca^{2+}$ stores using a combination of the ryanodine receptor agonist caffeine (10 mM) and the SERCA inhibitor CPA (30 μM) resulted in far less $Ca^{2+}$ release in mSTIM1$^{-/-}$ than in

WT myofibers, which indicates a substantial decrease in the pool of stored $Ca^{2+}$ in mSTIM1$^{-/-}$ myofibers (Fig. 4A and B). In addition, we found that SOCE was nearly absent from fibers of mSTIM1$^{-/-}$ mice compared to the robust $Ca^{2+}$ entry of WT fibers (Fig. 4A and C). We also noted a small but highly significant decrease in basal $Ca^{2+}$ levels in mSTIM1$^{-/-}$ compared to the levels in WT myofibers (Fig. 4D). These studies demonstrate that STIM1 is necessary to support SOCE in skeletal muscle.

To evaluate excitation contraction coupling (ECC), we assessed the ability of WT and mSTIM1$^{-/-}$ myofibers to release $Ca^{2+}$ from SR/ER $Ca^{2+}$ stores in response to electrical stimulation, a critical mechanism to release RYR1 stores. WT and mSTIM1$^{-/-}$ myofibers activated with single bursts of stimulation (50 Hz) over a range of pulse durations (200 ms to 5 s) exhibited no differences in peak $[Ca^{2+}]_c$, indicating that ECC was intact (Fig. 4E). STIM1 was recently implicated as an inhibitor of voltage-gated $Ca^{2+}$ currents through a direct interaction with Cav1.2 (17, 30). Given the importance of Cav1.1 in ECC in skeletal muscle, we measured voltage-gated $Ca^{2+}$ currents from WT and mSTIM1$^{-/-}$ myotubes after 9 days of differentiation. In contrast to the reported inhibition of $Ca^{2+}$ currents in smooth muscle and neurons, we found no differences in the voltage-dependent $Ca^{2+}$ currents between WT and mSTIM1$^{-/-}$ myotubes (Fig. 4F).

To this point, the results of our studies indicate that EC coupling is intact in muscle lacking SOCE. However, we found that activating myofibers with prolonged repetitive electrical stimulation protocols (2-s bursts at 50 Hz every 5 s) to mimic tonic stimulation revealed marked differences in the $Ca^{2+}$ signaling of mSTIM1$^{-/-}$ myofibers and WT myofibers (Fig. 5A). Whereas the $Ca^{2+}$ responses during such repetitive activity remained relatively sustained in the WT fibers, the responses from mSTIM1$^{-/-}$ myofibers were substantially attenuated. We next sought to determine whether the reduced responsiveness to tonic stimulation corresponded to altered growth signaling through AKT and ERK1/2. While tonic stimulation of isolated muscles from WT and mSTIM1$^{-/-}$ mice led to marked increases in phosphorylated AKT (p-AKT) and p-ERK1/2, the overall activation status of each of these pathways was comparatively diminished in mSTIM1$^{-/-}$ muscle (Fig. 5B and C). When considered together, the results of these $Ca^{2+}$-imaging studies demonstrate that STIM1 is required in skeletal muscle to maintain basal cytosolic and SR/ER $Ca^{2+}$ levels, as well as the $Ca^{2+}$ signals evoked by tonic electrical activity.

**STIM1 and $Ca^{2+}$-dependent signaling.** Pathways downstream of many growth factors are often influenced by cytosolic $Ca^{2+}$, raising the possibility that defects in STIM1-SOCE may impair growth factor signal transduction. Here, we investigated the activation state of signal transduction pathways, including calcineurin in mSTIM1$^{-/-}$ muscle (1, 6, 21). In particular, we found a greater fraction of the phosphorylated form of NFATC3 in the muscles of mSTIM1$^{-/-}$ mice than in those of WT mice, indicating that less NFATC3 was available for nuclear translocation in these muscles (Fig. 6A). PPARγ, muscle enhancer factor 2C (MEF2C), and PPAR-γ coactivator (PGC-1α and PGC-1β) are important transcription factors that regulate skeletal muscle differentiation and metabolism (9). We also found marked reductions in these metabolic transcription factors in the muscles of mSTIM1$^{-/-}$ mice (Fig. 6B). A second NFAT isoform found in muscle, NFATc1, was markedly reduced in the muscles of mSTIM1$^{-/-}$ mice compared to its levels in WT littermates (Fig. 6B). Interestingly, it is known that calcineurin regulatory elements in the NFATc1 promoter control NFATc1 expression and, therefore, link NFATc1 to $Ca^{2+}$ (34). These data indicate that STIM1-$Ca^{2+}$ signaling is needed to support muscle differentiation associated with calcineurin/NFAT signaling in the mSTIM1$^{-/-}$ muscle. In fact, we found marked reductions in the expression of myoglobin and SERCA1, whose genes are established target genes for the calcineurin/NFAT signaling (Fig. 6B). We next sought to determine whether a $Ca^{2+}$-independent form of calcineurin could rescue the signaling elements altered in the mSTIM1$^{-/-}$ muscle. While the STIM1-deficient myotubes have decreased activation states of AKT and ERK1/2 compared to those of WT myotubes, adenoviral delivery of constitutively active calcineurin to these myotubes led to marked increases in the activation states of AKT and ERK1/2, as well as increased expression of MEF2 and myoglobin (Fig. 6C). We interpret the results of these studies as evidence that at least some of the defects observed in muscle lacking STIM1-SOCE could be recovered by enhancing calcineurin activity in primary cultured myotubes.

## DISCUSSION

In the present work, we provide evidence that the ER $Ca^{2+}$ sensor STIM1 has a fundamental role in postnatal skeletal muscle growth and survival. According to our model, STIM1 is required to coordinate the levels of $Ca^{2+}$ in the cytosol and the SR, the main $Ca^{2+}$ storage organelle in muscle. We show that in STIM1-deficient muscle, both basal cytosolic and ER/SR $Ca^{2+}$ levels are reduced at rest and that $Ca^{2+}$ transients evoked by tonic electrical stimulation show a decrement over time. To account for these dramatic effects, we show that STIM1 is necessary to activate $Ca^{2+}$ entry and regulate the expression of SERCA1. In this way, STIM1 is important for maintaining the $Ca^{2+}$ equilibrium within the cell that is fundamental to growth signal transduction cascades.

At birth, the muscles of mSTIM1$^{-/-}$ mice are indistinguishable from those of WT littermates; however, after several days of postnatal life (P10 to P21), these mice exhibit severe signs of distress and reduced muscle mass that include a reduction in myonuclear accretion and failed expansion of the myodomain. To provide a mechanistic basis for the diminished muscle mass, we show that the STIM1-deficient muscles exhibit marked reductions in the activation state of many growth signaling pathways, most notably those governed by calcineurin, p38 MAP kinase, AKT, and ERK1/2. In fact, these mice are severely underweight and die prematurely, much as observed for global STIM1 knockout mice. We therefore conclude that STIM1 in skeletal muscle serves as a central regulator of $Ca^{2+}$ signaling that resides upstream of muscle growth signaling and is important in the adaptation events associated with greater locomotor and metabolic demand occurring during the neonatal period.

Here, we propose that the effects of STIM1 on SOCE and SERCA1 activity in skeletal muscle can be readily distinguished from large $Ca^{2+}$ signaling events associated with ECC (Cav1.1 and RYR1). In fact, we show that the levels of $Ca^{2+}$ release in response to membrane depolarization and the $Ca^{2+}$ currents attributed to Cav1.1 channels were equivalent in muscles of mSTIM1$^{-/-}$ and WT mice. These data are consistent with the notion that even though SR/ER $Ca^{2+}$ stores are reduced in mSTIM1$^{-/-}$ muscle, $Ca^{2+}$ release via ECC remains intact. Given that a single twitch contraction releases approximately 10 to 20% of available $Ca^{2+}$ from the SR/ER (23, 24), we would not anticipate this decrease in SR/ER $[Ca^{2+}]_c$ to be sufficient to activate STIM1-SOCE. How-

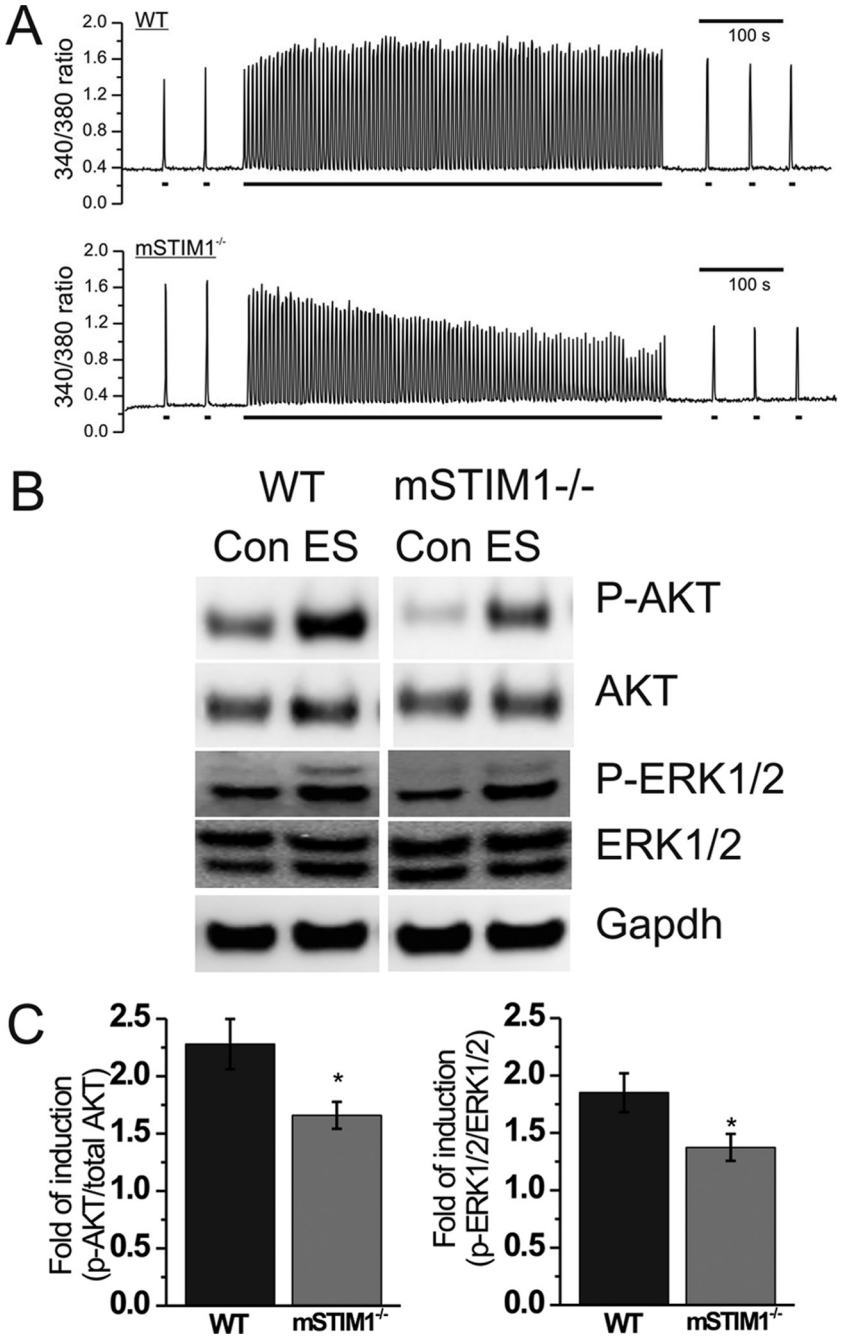


**FIG 5** mSTIM1$^{-/-}$ myofiber and muscle responses to sustained electrical activity. (A) $Ca^{2+}$ transients generated by repeated bursts of electrical activity in WT (top) and mSTIM1$^{-/-}$ (bottom) FDB myofibers. Fibers were repeatedly stimulated with bursts (2 s at 50 HZ, every 5 s [long bar]) for 13 min. (B) The phosphorylation of AKT and p44/42 was measured by immunoblotting of hind-limb muscles following repeated electrical stimulation (500 ms at 50 Hz, every 5 s) of hind limbs for 30 min (ES) and in the absence of electrical stimulation (Con [control]). (C) Relative ratios of phosphorylated to total AKT and p44/42 in hind-limb muscles. Protein loading was normalized by immunoblotting for actin. *, $P < 0.05$.

ever, we show that the $Ca^{2+}$ signals evoked by trains of electrical stimulation in mSTIM1$^{-/-}$ muscle fibers were greatly attenuated compared to those in WT muscle fibers. These findings indicate that myofibers require SERCA1 activity and SOCE during sustained stimulation, both of which are diminished in the mSTIM1$^{-/-}$ mice. Whether $Ca^{2+}$ entry during repetitive stimulations is specific to the exon 11 spliced variant of STIM1 or is a more generalized mechanism for SOCE in muscle remains to be determined (2). Moreover, these results from mSTIM1$^{-/-}$ myofibers bear striking similarities to the results of studies conducted on WT myofibers stimulated in the absence of external $Ca^{2+}$ and in myofibers with reduced $Ca^{2+}$-buffering capacity (24, 26, 32) (P. Rosenberg and E. A. Finch, unpublished results). These findings highlight that STIM1 has a fundamental role in coordinating $Ca^{2+}$ signaling in skeletal muscle.

We also provide evidence that $Ca^{2+}$ signaling during repetitive

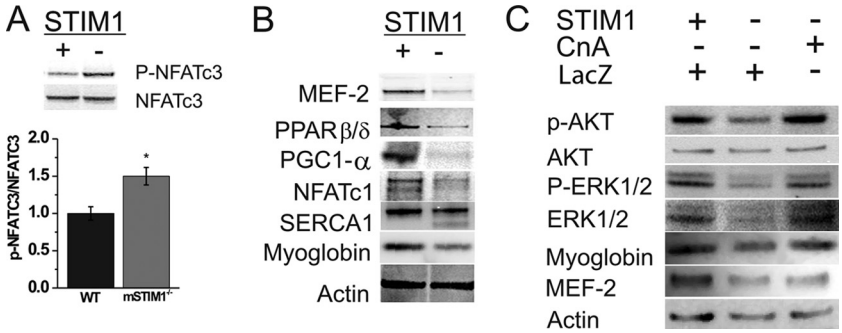


**FIG 6** Impaired hypertrophic signaling in muscles of mSTIM1$^{-/-}$ mice. (A) Representative immunoblots for p-NFATC3 and NFATC3 in protein lysates from WT and mSTIM1$^{-/-}$ muscle (top). Ratio between phospho-NFATc3 and total NFATc3 in WT and mSTIM1$^{-/-}$ muscles reveals decreased phosphorylation in mSTIM1$^{-/-}$ muscle (bottom). (B) Representative immunoblots for MEF-2, PPAR-β/δ, PGC-1α, NFATC1, SERCA1, and myoglobin protein levels in WT and mSTIM1$^{-/-}$ muscle lysates. (C) Overexpression of constitutively active calcineurin (CnA) in the primary cultured STIM1$^{-/-}$ myotubes rescues the hypertrophic signaling pathway. Expression levels of p-ERK1/2, ERK1/2, p-AKT, AKT, myoglobin, and MEF-2 and actin were measured in WT myotubes, mSTIM1$^{-/-}$ myotubes (transduced with adenovirus carrying beta-galactosidase), and mSTIM1$^{-/-}$ myotubes (transduced with an adenovirus that overexpresses constitutively active calcineurin) (MOI = 50 for each). Each experiment was repeated three times using four animals from each genotype. *, $P < 0.05$.

electrical activity plays an important role in the activation of growth signaling pathways. Deletion of STIM1 impairs growth signaling, including that of AKT and ERK1/2. Given the role of these kinases in muscle growth and performance, our results suggest that STIM1 links changes in AKT and ERK1/2 signaling to altered locomotor activity. The deficits in $Ca^{2+}$ release during repetitive stimulation discussed above are consistent with the idea that multiple signal transduction cascades associated with growth signaling (calcineurin, AKT, and ERK1/2) were diminished in muscles of mSTIM1$^{-/-}$ mice. STIM1-dependent $Ca^{2+}$ signaling is thus a key factor to perpetuating $Ca^{2+}$ oscillations which are then decoded by signal transduction pathways. We propose that STIM1 is critical to the $Ca^{2+}$-rich environment of the myofiber during neonatal growth in order to match the anabolic demand associated with muscle growth and that STIM1-$Ca^{2+}$ signaling is therefore required during neonatal muscle development in order to enable the $Ca^{2+}$ signaling required to meet various environmental challenges.

In conclusion, our results demonstrate that STIM1-SOCE has a critical cellular function during skeletal muscle growth and differentiation. Given the fundamental role of SOCE in immune cells, it was rather unexpected that STIM1-SOCE would have such an important role in skeletal muscle $Ca^{2+}$ signaling. For both immune cells and skeletal muscle, STIM1 mediates an essential molecular mechanism to maintain repetitive $Ca^{2+}$ oscillations and transients. In this way, STIM1-$Ca^{2+}$ signals are needed to maintain signal transduction and the activation of cell growth pathways. Here, we show that mice with a conditional deletion of STIM1 from their skeletal muscle manifest a congenital myopathy that resembles the condition of humans harboring mutations in STIM1. Growing evidence from several groups indicates that SOCE is subject to alteration in other skeletal myopathies, including muscular dystrophy and sarcopenia of aging (5, 7, 12, 33). Whether this $Ca^{2+}$ entry is adaptive or not remains to be determined. We speculate that STIM1-SOCE may also be important for activating growth and differentiation pathways in regenerating muscle and that it is therefore an adaptive response. Thus, our results raise the possibility that enhancing STIM1-SOCE $Ca^{2+}$ signaling may represent a novel therapeutic strategy for disorders associated with muscle atrophy.

## ACKNOWLEDGMENTS

Sources of funding include grants from NIH (R01-HL093470 to P.R. and T32 HL007101 to T.L.) and an MDA research award (P.R.).

## REFERENCES

1. **Bodine SC, et al.** 2001. Akt/mTor pathway is a crucial regulator of skeletal muscle hypertrophy and can prevent muscle atrophy in vivo. Nat. Cell. Biol. **3**:1014–1019.
2. **Darbellay B, Arnaudeau S, Bader CR, Konig S, Bernheim L.** 2011. STIM1L is a new actin-binding splice variant involved in fast repetitive Ca2+ release. J. Cell Biol. **194**:335–346.
3. **Darbellay B, et al.** 2009. STIM1- and Orai1-dependent store-operated calcium entry regulates human myoblast differentiation. J. Biol. Chem. **284**:5370–5380.
4. **De Windt LJ, Lim HW, Haq S, Force T, Molkentin JD.** 2000. Calcineurin promotes protein kinase C and c-Jun NH2-terminal kinase activation in the heart. Cross-talk between cardiac hypertrophic signaling pathways. J. Biol. Chem. **275**:13571–13579.
5. **Duke AM, Hopkins PM, Calaghan SC, Halsall JP, Steele DS.** 2010. Store-operated Ca2+ entry in malignant hyperthermia-susceptible human skeletal muscle. J. Biol. Chem. **285**:25645–25653.
6. **Dunn SE, Simard AR, Prud'homme RA, Michel RN.** 2002. Calcineurin and skeletal muscle growth. Nat. Cell Biol. **4**:E46–E47.
7. **Edwards JN, et al.** 2010. Upregulation of store-operated Ca2+ entry in dystrophic mdx mouse muscle. Am. J. Physiol **299**:C42–C50.
8. **Feske S, et al.** 2006. A mutation in Orai1 causes immune deficiency by abrogating CRAC channel function. Nature **441**:179–185.
9. **Gaudel C, Schwartz C, Giordano C, Abumrad NA, Grimaldi PA.** 2008. Pharmacological activation of PPARbeta promotes rapid and calcineurin-dependent fiber remodeling and angiogenesis in mouse skeletal muscle. Am. J. Physiol. Endocrinol. Metab. **295**:E297–E304.
10. Reference deleted.
11. Reference deleted.
12. **Launikonis BS, Murphy RM, Edwards JN.** 2010. Toward the roles of store-operated Ca2+ entry in skeletal muscle. Pflugers Arch. **460**:813–823.
13. **Li S, et al.** 2005. Requirement for serum response factor for skeletal muscle growth and maturation revealed by tissue-specific gene deletion in mice. Proc. Natl. Acad. Sci. U. S. A. **102**:1082–1087.
14. **Liou J, et al.** 2005. STIM is a Ca2+ sensor essential for Ca2+-store-depletion-triggered Ca2+ influx. Curr. Biol. **15**:1235–1241.
15. Reference deleted.
16. **Oh-Hora M, et al.** 2008. Dual functions for the endoplasmic reticulum calcium sensors STIM1 and STIM2 in T cell activation and tolerance. Nat. Immunol. **9**:432–443.
17. **Park CY, Shcheglovitov A, Dolmetsch R.** 2010. The CRAC channel

activator STIM1 binds and inhibits L-type voltage-gated calcium channels. Science **330**:101–105.
18. **Picard C, et al.** 2009. STIM1 mutation associated with a syndrome of immunodeficiency and autoimmunity. N. Engl. J. Med. **360**:1971–1980.
19. Reference deleted.
20. **Raney MA, Turcotte LP.** 2008. Evidence for the involvement of CaMKII and AMPK in Ca2+-dependent signaling pathways regulating FA uptake and oxidation in contracting rodent muscle. J. Appl. Physiol. **104**:1366–1373.
21. **Rommel C, et al.** 2001. Mediation of IGF-1-induced skeletal myotube hypertrophy by PI(3)K/Akt/mTOR and PI(3)K/Akt/GSK3 pathways. Nat. Cell Biol. **3**:1009–1013.
22. **Roos J, et al.** 2005. STIM1, an essential and conserved component of store-operated Ca2+ channel function. J. Cell Biol. **169**:435–445.
23. **Royer L, Rios E.** 2009. Deconstructing calsequestrin. Complex buffering in the calcium store of skeletal muscle. J. Physiol. **587**:3101–3111.
24. **Royer L, et al.** 2010. Paradoxical buffering of calcium by calsequestrin demonstrated for the calcium store of skeletal muscle. J. Gen. Physiol. **136**:325–338.
25. **Shefer G, Yablonka-Reuveni Z.** 2005. Isolation and culture of skeletal muscle myofibers as a means to analyze satellite cells. Methods Mol. Biol. **290**:281–304.
26. **Shin DW, et al.** 2003. A retrograde signal from calsequestrin for the regulation of store-operated Ca2+ entry in skeletal muscle. J. Biol. Chem. **278**:3286–3292.
27. **Stiber J, et al.** 2008. STIM1 signalling controls store-operated calcium entry required for development and contractile function in skeletal muscle. Nat. Cell Biol. **10**:688–697.
28. **Stiber JA, et al.** 2005. Homer modulates NFAT-dependent signaling during muscle differentiation. Dev. Biol. **287**:213–224.
29. **Vig M, et al.** 2008. Defective mast cell effector functions in mice lacking the CRACM1 pore subunit of store-operated calcium release-activated calcium channels. Nat. Immunol. **9**:89–96.
30. **Wang Y, et al.** 2010. The calcium store sensor, STIM1, reciprocally controls Orai and CaV1.2 channels. Science **330**:105–109.
31. **Zhang SL, et al.** 2005. STIM1 is a Ca2+ sensor that activates CRAC channels and migrates from the Ca2+ store to the plasma membrane. Nature **437**:902–905.
32. **Zhao X, et al.** 2010. Increased store-operated Ca2+ entry in skeletal muscle with reduced calsequestrin-1 expression. Biophys. J. **99**:1556–1564.
33. **Zhao X, et al.** 2008. Compromised store-operated Ca2+ entry in aged skeletal muscle. Aging Cell **7**:561–568.
34. **Zhou B, et al.** 2002. Regulation of the murine Nfatc1 gene by NFATc2. J. Biol. Chem. **277**:10704–10711.